

Development of [¹⁸F]FPy-WL12 as a PD-L1 Specific PET Imaging Peptide

Wojciech G. Lesniak, PhD¹, Ronnie C. Mease, PhD^{1,2}, Samit Chatterjee, PhD¹, Dhiraj Kumar, PhD¹, Ala Lisok, MA¹, Bryan Wharram, MS¹, Venkateswara Rao Kalagadda, PhD¹, Leisha A. Emens, MD, PhD², Martin G. Pomper, MD, PhD^{1,2}, and Sridhar Nimmagadda, PhD^{1,2} 

Abstract

Expression of programmed cell death ligand 1 (PD-L1) within tumors is an important biomarker for guiding immune checkpoint therapies; however, immunohistochemistry-based methods of detection fail to provide a comprehensive picture of PD-L1 levels in an entire patient. To facilitate quantification of PD-L1 in the whole body, we developed a peptide-based, high-affinity PD-L1 imaging agent labeled with [¹⁸F]fluoride for positron emission tomography (PET) imaging. The parent peptide, WL12, and the nonradioactive analog of the radiotracer, ¹⁹FPy-WL12, inhibit PD-1/PD-L1 interaction at low nanomolar concentrations (half maximal inhibitory concentration [IC₅₀], 26-32 nM). The radiotracer, [¹⁸F]FPy-WL12, was prepared by conjugating 2,3,5,6-tetrafluorophenyl 6-[¹⁸F]fluoronicotinate ([¹⁸F]FPy-TFP) to WL12 and assessed for specificity in vitro in 6 cancer cell lines with varying PD-L1 expression. The uptake of the radiotracer reflected the PD-L1 expression assessed by flow cytometry. Next, we performed the in vivo evaluation of [¹⁸F]FPy-WL12 in mice bearing cancer xenografts by PET imaging, ex vivo biodistribution, and blocking studies. In vivo data demonstrated a PD-L1-specific uptake of [¹⁸F]FPy-WL12 in tumors that is reduced in mice receiving a blocking dose. The majority of [¹⁸F]FPy-WL12 radioactivity was localized in the tumors, liver, and kidneys indicating the need for optimization of the labeling strategy to improve the in vivo pharmacokinetics of the radiotracer.

Keywords

PD-L1, immunotherapy, molecular imaging, positron emission tomography

Introduction

Cancer cells develop multiple mechanisms to evade immune recognition and create a microenvironment that sustains immune tolerance.¹ One of them involves interactions of immune checkpoint protein programmed cell death ligand-1 (PD-L1), expressed in tumors, with programmed cell death protein 1 (PD-1), present on immune cells, that lead to their deactivation.² PD-L1 is expressed in many tumor types, and its levels in the tumors assessed by immunohistochemistry may be used for patient stratification for therapy involving inhibition of PD-1/PD-L1 immune check point.² Two immunohistochemistry-based PD-L1 companion diagnostic tests received Food and Drug Administration approval to guide therapies targeted against PD-L1 and its receptor PD-1.³ Those tests, however, do not fully capture the inter- and intratumoral heterogeneity in PD-L1 expression that have implications in guiding therapy.⁴ Noninvasive imaging technologies, particularly positron emission tomography (PET),

have the potential to quantify total PD-L1 levels in all the lesions provided that a high-affinity molecularly targeted imaging agent is available.⁵

Significant efforts have been invested in developing PD-L1-targeted imaging agents. Radiolabeled antibodies,⁶⁻¹¹ high-affinity ectodomains derived from PD-1,¹² and adnectin-derived^{13,14} small proteins have been investigated as nuclear imaging agents. All those agents have shown promise in

¹ Russell H. Morgan Department of Radiology and Radiological Science, Johns Hopkins University, Baltimore, MD, USA

² Sidney Kimmel Comprehensive Cancer Center, Bloomberg ~ Kimmel Institute for Cancer Immunotherapy, Johns Hopkins University, Baltimore, MD, USA

Submitted: 02/01/2019. Revised: 13/03/2019. Accepted: 15/04/2019.

Corresponding Author:

Sridhar Nimmagadda, Johns Hopkins Medical Institutions, 1550 Orleans Street, CRB II, #491, Baltimore, MD 21287, USA.

Email: snimmag1@jhmi.edu



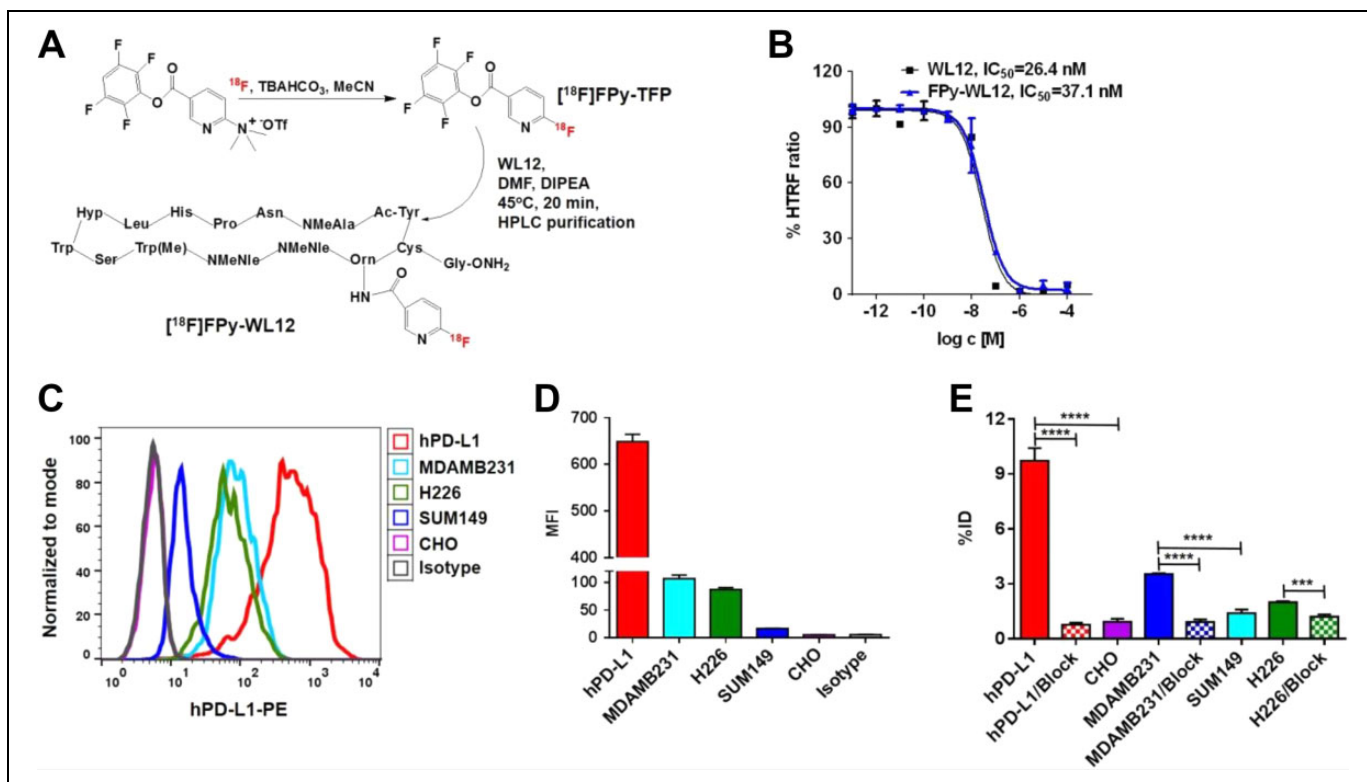


Figure 1. Radiofluorination of WL12 and in vitro evaluation. A, schematic depiction of WL12 radiofluorination achieved via selective acylation of ornithine side chain primary amine with prosthetic group [18F]FPy-TFP. B, Inhibition of PD1–PD-L1 interaction by unmodified WL12 peptide and nonradioactive analog, 19Fpy-WL12, as measured by FRET. C, Flow cytometry analysis of various cell lines for cell surface PD-L1 expression. D, Representative mean fluorescence intensity (MFI) values for PE-conjugated anti-human PD-L1 antibody binding to various cell lines. E, In vitro binding of [18F]FPy-WL12 to hPDL1, CHO, MDAMB231, SUM149, H226, and H1155 cells incubated with 37 kBq (1 μ Ci)/100 μ L of [18F]WL12 at 37 $^{\circ}$ C for 1 hour. Data are represented as percentage of incubated dose (%ID) per million cells, **** $P < .0001$, *** $P < .001$.

detecting PD-L1 expression in preclinical cancer models. Despite those developments, there is a need for radiotracers labeled with readily available positron-emitting radionuclides, such as ¹⁸F or ⁶⁸Ga, that allow imaging of PD-L1 within 60 to 120 minutes after injection that is more adequate to clinical workflow. In a recent study, we demonstrated that a human PD-L1-specific, 14-amino acid cyclic peptide conjugated with 2,2',2''-(10-(2,6-dioxotetrahydro-2H-pyran-3-yl)-1,4,7,10-tetraazacyclododecane-1,4,7-triyl)triacetic acid (DOTAGA) and radiolabeled with ⁶⁴Cu or ⁶⁸Ga can be used to generate high-contrast images of PD-L1 expression in tumors by PET imaging and to assess the target engagement of PD-L1 therapeutics.¹⁵⁻¹⁷ Because of the greater availability of ¹⁸F and its well-suited properties for PET imaging, we pursued the development and evaluation of a radiofluorinated analog of WL12.

Here, we report the preparation of a radiofluorinated analog of WL12 using 2,3,5,6- tetrafluorophenyl 6-[18F]fluoronicotinate. We describe the evaluation of the resulting radiotracer, [18F]FPy-WL12, in vitro and in vivo, in 6 cancer cell lines with a range of levels of PD-L1 expression. Our results demonstrate that [18F]FPy-WL12 specifically detects PD-L1 expression in tumors and that further optimization of the radiotracer is needed to improve the in vivo distribution and image contrast.

Materials and Methods

Chemicals

The PD-L1-binding peptide, WL12 (sequence shown in Figure 1A), was custom synthesized by CPC Scientific (Sunnyvale, California) with >95% purity. 6-Fluoronicotinic acid was purchased from Combi-Blocks (San Diego, California). [18F]Fluoride was produced by 18-MeV proton bombardment of a high-pressure [18O]H₂O target using a General Electric PETtrace biomedical cyclotron (GE Healthcare, Chicago, Illinois). N,N,N-trimethyl-5-((2,3,5,6-tetrafluorophenoxy)carbonyl)pyridine-2-aminium tri-fluoromethane sulfonate was prepared as reported previously.¹⁸ All other chemicals were purchased from Sigma-Aldrich (Milwaukee, Wisconsin) or Thermo Fisher Scientific (Waltham, Massachusetts) unless otherwise specified.

All cell culture-related reagents were purchased from Invitrogen, unless otherwise specified. Polyclonal anti-human IgG-Eu3+Cryptate (catalog # 61HFCKLA) and XL665- conjugated mouse monoclonal anti-6Histidine antibody (catalog # 61HISXLA) were purchased from Cisbio Assays (Bedford, Massachusetts). Recombinant Human PD-1 Fc chimera Protein (catalog #1086-PD-050) and recombinant human

PD-L1(B7-H1)-His-tag protein (catalog #9049-B7) were obtained from R&D systems (Minneapolis, Minnesota).

Electrospray ionization mass spectra were obtained on a Bruker Daltonics Esquire 3000 Plus Spectrometer. Semi-preparative high-performance liquid chromatography (HPLC) was performed using a system containing 2 Agilent ProStar HPLC pumps and an Agilent 1260 Infinity Diode Array detector controlled by Open Lab Software, version A.01.05 (Santa Clara, California). Radio-HPLC was performed on a Varian ProStar system (Palo Alto, California) equipped with a Varian ProStar 325 ultraviolet (UV)-visible (Vis) variable wavelength detector and a BioScan Flow-Count in-line radioactivity detector (Washington, District of Columbia), all controlled by Galaxie software (Varian, Inc. Palo Alto, California). The specific activity was calculated as the ratio of the radioactivity eluting at the retention time of the product during the semi-preparative HPLC purification to the mass corresponding to the area under the UV peak.

Chemistry

2,3,5,6-Tetrafluorophenyl 6-fluoronicotinate. To a solution of 1.76 g (12.4 mM) 6-fluoronicotinic acid dissolved in 40-mL dry tetrahydrofuran (THF) was added a solution of 2.7 g (11 mM) 2,3,5,6-tetrafluorophenol dissolved in 10 mL dry THF. To this mixture was added, in small portions, a solution consisting of 2.57 g (12.4 mM) dicyclohexycarbodiimide (DCC) dissolved in 15 mL dry THF and allowed to stir at room temperature for 6 days. The reaction was filtered to remove the white biproduct, dicyclohexylurea. The filtrate was concentrated to a residue, dissolved in dichloromethane, and allowed to stand in order to precipitate more dicyclohexylurea. The procedure was repeated twice using a 10/1 solution of hexanes/ethyl acetate to remove all the dicyclohexylurea. The final filtrate was concentrated, redissolved in 30mL of 10/1 solution of hexanes/ethyl acetate, and purified on a silica gel column using the same hexane/ethyl acetate mobile phase to give 1.88g of a thick colorless oil which solidified. $^1\text{H-nmr}$ (400MHz, CDCl_3) δ 9.109 (s, 1H), 8.592 (m, 1H), 7.155 (dd, $J = 3.2, 8.4\text{Hz}$, 1H), 7.108 (m, 1H). $^1\text{H-nmr}$ (500MHz CDCl_3) 9.10 (dt, $J_t = 0.5\text{Hz}, J_d = 2.5\text{Hz}$, 1H), 8.57 (ddd, $J_1 = 2.5\text{Hz}, J_2 = 7.4\text{Hz}, J_3 = 8.6\text{Hz}$, 1H), 7.13 ddd, $J_1 = 0.5\text{Hz}, J_2 = 3.0\text{Hz}, J_3 = 8.6\text{Hz}$, 1H), 7.09 (tt, $J_1 = 7.1\text{Hz}, J_2 = 9.9\text{Hz}$, 1H).

FPy-WL12. Five mg of WL12 (2.51×10^{-6} M) was reacted with 3.6 mg of 2,3,5,6- tetrafluorophenyl 6-fluoronicotinate (1.25×10^{-5} M) in 1 mL of dimethylformamide (DMF) in the presence of 2 M equivalents of diisopropylethyl amine for 30 minutes at 60°C to provide FPy-WL12 (Supplementary Figure S1A). The resulting peptide was purified on a Reverse phase (RP) HPLC using a 10×250 mm, 5- μ Luna C18 column (Phenomenex, Torrance, California) using an acetonitrile/water gradient with 0.1% trifluoroacetic acid (TFA). The elution conditions were 35% to 75% acetonitrile with 0.1%TFA at a flow rate of 5 mL/min in 25 minutes (Supplementary Figure S1B) with water + 0.1% TFA as co-solvent. FPy-WL12 was collected at ~ 20 minutes of elution, and following evaporation, the resulting residue was

dissolved in deionized water and lyophilized, yielding 4.5 mg of a white powder (yield 89%). electrospray ionization mass spectrometry (ESI-MS) calcd for $[\text{M}+\text{H}]^+$ 2005.0, found 2004.7; calc for $[\text{M}+2\text{H}]^2 = 1003.0$, found 1003.4.

Radiochemistry

2,3,5,6-Tetrafluorophenyl 6- ^{18}F fluoronicotinate. 2,3,5,6-Tetrafluorophenyl 6- ^{18}F fluoronicotinate was prepared by the procedure of Basuli et al, with a minor modification.¹⁹ Fluorine-18 target water (87-100mCi) was diluted to 4 mL with high-purity water (TraceSELECT, Honeywell) and passed through a Chromafix 30-PS- HCO_3 anion exchange cartridge pretwetted with 2 mL of TraceSELECT water. The cartridge was washed with 4 mL anhydrous acetonitrile and dried for 2 minutes by passing a stream of argon gas. The cartridge was then slowly eluted with a solution consisting of 5 to 11 mg of N,N,N-trimethyl-5- ((2,3,5,6-tetrafluorophenoxy)carbonyl)-pyridine-2-aminium trifluoromethane sulfonate, dissolved in 1 mL of 4:1 t-butanol/acetonitrile. This was diluted to 2 mL with water and purified by RP-radio-HPLC (10×250 mm, 10 μ , Luna C18 column; Phenomenex; solvent A 100% water +0.1% TFA; solvent B 100% acetonitrile +0.1% TFA; gradient 80% A to 20% A over 30 minutes; flow rate 4 mL/min). The desired 2,3,5,6-tetrafluorophenyl 6- ^{18}F fluoronicotinate (24-41 mCi) was collected at $R_t = 28$ minutes, diluted with water to 20 mL, loaded onto a preactivated (20mL acetonitrile followed by 20mL water) Waters C18 Sep-Pak Plus cartridge (Waters, Milford, Massachusetts), and cartridge was dried by passing argon for several minutes. A sodium sulfate drying cartridge (Grace-Davison, Columbia, Maryland) was attached to the C18 cartridge and the C18 cartridge eluted with 2 mL of methylene chloride through the drying cartridge.

^{18}F FPy-WL12. To the methylene chloride solution of 2,3,5,6-tetrafluorophenyl 6- ^{18}F fluoronicotinate was added 100 μL DMF, and this was concentrated to approximately 100 μL under a stream of argon. To this was added a solution consisting of 0.1 to 0.14 mg (50-70 nM) WL12 in 50 μL DMF and 4 μL di-isopropylethyl amine. The reaction mixture was heated at 45°C for 20 minutes, diluted with water, and purified by RP radio-HPLC (10×250 mm, 10 μ , Luna C18 column; solvent A 100% water +0.1% TFA, solvent B 100% acetonitrile +0.1% TFA; Gradient 65% A to 25% A over 25 minutes; flow 5 mL/m). The desired ^{18}F FPy-WL12 (2.8-7.8 mCi) was collected at $R_t = 11$ minutes. Unlabeled WL12 eluted at 7.5 minutes. ^{18}F FPy-WL12 in HPLC mobile phase was evaporated under reduced pressure, reconstituted in saline containing 5% dimethylsulfoxide and 2 drops of Tween 20, and diluted with saline for in vitro and in vivo studies.

Programmed cell death ligand 1-PD-1 binding inhibition assay. Competitive PD-L1/PD-1 inhibition assay was performed as described.¹⁵ Briefly, PD-L1- His-tag (80 nM final) in 10 μL assay buffer was preincubated for 15 minutes with varying concentrations WL12 or FPy-WL12 ranging from 1 pM to

1 mM. This was followed by addition of 5 μL of assay buffer containing PD-1-Ig (final concentration 20 nM) and incubated for 15 minutes. Then, 5 μL of assay buffer with IgG-Eu (final concentration 2 nM) and anti-6HIS-XL665 (final concentration 40 nM) was added. After 1 hour of incubation at room temperature, the plate was read on a Perkin Elmer Victor3 1420 multilabel counter (Waltham, Massachusetts). The half maximal inhibitory concentration (IC₅₀) and *K_i* values were derived by fitting the data to a sigmoidal dose-response curve and the Cheng-Prusoff equation with derived *K_d* = 70 nM for PD-L1, respectively. Experiments were carried out in triplicates.

Cell Lines

Cell lines NCI-H226 (LSCC), NCI-H1155 (NSCLC), MDAMB231 (TNBC), and CHO-K1, (henceforth referred to as H226, H1155, MDAMB231, and CHO, respectively) were purchased from the American Type Culture Collection (ATCC) and passaged for fewer than 3 months after which new cultures were initiated from vials of frozen cells. The SUM149 (TNBC) cell line was kindly provided by Dr Stephen P. Ethier, Medical University of South Carolina, and authenticated by STR profiling at the Johns Hopkins genetic resources facility. SUM149 cells were maintained in Ham's F-12 medium with 5% fetal bovine serum (FBS), 1% P/S and 5 $\mu\text{g}/\text{mL}$ insulin, and 0.5 $\mu\text{g}/\text{mL}$ hydrocortisone. All other cell lines were cultured in ATCC-recommended media in an incubator at 37°C in an atmosphere containing 5% CO₂. The CHO cell line stably expressing human PD-L1 (hPD-L1) was generated in our laboratory and maintained in F-12K medium with 10% FBS, 1% P/S, and 2 mg/mL G418.⁸

[¹⁸F]FPy-WL12 in vitro uptake assay. In vitro binding of [¹⁸F]FPy-WL12 to hPD-L1, CHO, MDAMB231, SUM149, H226, and H1155 cells was examined using 1 \times 10⁶ cells. Cells were detached using nonenzymatic cell dissociation buffer (Gibco, Cat no: 13151-014), suspended in phosphate-buffered saline (PBS) buffer containing 2 mM of EDTA and 1% of FBS, and incubated with 1 μCi of the radiotracer for 1 hour at 37°C. After incubation, cells were washed 3 times with cold PBS and bound radioactivity counted on an automated gamma counter (1282 Compugamma CS; Pharmacia/LKB Nuclear, Inc, Gaithersburg, Maryland). To demonstrate PD-L1-specific binding of [¹⁸F]FPy-WL12, blocking was carried out with 1 μM unmodified WL12. All the in vitro uptake studies were performed in triplicate for each cell line and repeated 3 times.

Animal Models

Animal studies were performed according to the protocols approved by the JHU Animal Care and Use Committee (ACUC). Six- to eight-week old, female, nonobese diabetic severe combined immunodeficient γ (NSG) mice were obtained from the JHU Immune Compromised Animal Core (Baltimore, Maryland). Mice were implanted subcutaneously in the upper flanks with hPD-L1 (10 \times 10⁶), CHO (10 \times 10⁶),

H226 (2 \times 10⁶), H1155 (2 \times 10⁶), MDAMB231 (2 \times 10⁶), and SUM149 (2 \times 10⁶) cells in 100 μL of HBSS containing 50% matrigel (Corning). Mice were used for imaging or *ex vivo* biodistribution experiments when the tumors reached a volume of 200-300 mm³.

Positron Emission Tomography-Computed Tomography Imaging of Mouse Xenografts

NSG mice bearing CHO/hPD-L1, MDAMB231, or H226 tumors were injected with \sim 7.4 mBq (200 μCi) of [¹⁸F]FPy-WL12 in 200 μL of saline intravenously (n = 3). The PET images were collected in 2-bed positions at 5 minutes per bed in an ARGUS small-animal PET/computed tomography (CT) scanner (Sedecal, Madrid, Spain). A CT scan (512 projections) was performed at the end of each PET scan for anatomical coregistration. Mice were anesthetized under 3% and maintained at 1.5% isoflurane during scanning. The PET data were reconstructed using the 2-dimensional ordered subsets expectation maximization algorithm (2D-OSEM) and corrected for dead time and radioactive decay. The %ID per cm³ values were calculated based on a calibration factor obtained from a known radioactive quantity. Final data visualization and image generation were accomplished using Amira (FEI, Hillsboro, Oregon).

Ex Vivo Biodistribution

Biodistribution studies were carried out at various time points in NSG mice bearing CHO/hPD-L1 (10, 60, and 120 minutes), MDAMB231 (60 and 120 minutes), SUM 149 (120 minutes), and H226 (120 minutes) xenografts to confirm PET imaging results. Mice were injected intravenously with 740 kBq (in 200 μL) of [¹⁸F]FPy-WL12, sacrificed at the specified time, and blood, tumors, and selected tissues were harvested and weighed. The radioactivity in collected samples was measured in a Perkin Elmer-2480 Automatic Gamma Counter (Perkin Elmer, Waltham, Massachusetts). To demonstrate the in vivo specificity, a 50- μg blocking dose of WL12 was co-injected with [¹⁸F]FPy-WL12. To calculate the percentage of injected dose per gram of tissue (%ID/g), radioactive standards in triplicate were counted with the tissues. Biodistribution data shown is mean \pm the standard error of the mean (SEM).

Data Analysis

Unpaired 2-tailed *t* test using the Prism 6 Software (GraphPad) was used for statistical analysis. *P* values <0.05 were considered to be significant.

Results

Synthesis of FPy-WL12 and [¹⁸F]FPy-WL12

Nonradioactive ¹⁹FPy-WL12 was prepared in 89% yield by conjugation of 2,3,5,6-tetrafluorophenyl 6-fluoronicotinate to WL12. [¹⁸F]FPy-WL12 was prepared in nondecay-corrected

yield of $5.1\% \pm 3.1\%$ ($n = 3$) from [^{18}F]fluoride by synthesizing 2,3,5,6-tetrafluorophenyl 6-[^{18}F]fluoronicotinate followed by conjugation to WL12 (Figure 1A). The specific activity achieved was 105 ± 54 Ci/mM with radiochemical purity $>95\%$.

WL12 and Fpy-WL12 Exhibit High Affinity to PD-L1

To test the binding affinity of WL12 and ^{19}F Py-WL12 to PD-L1, PD-1 binding to PD-L1 was assessed by Fluorescence Resonance Energy Transfer (FRET) in the presence of WL12 and ^{19}F Py-WL12 (Figure 1B). The binding isotherm obtained for both peptides showed a concentration-dependent inhibition with the half maximal inhibitory concentration (IC_{50}) of 26.4 nM, (95% confidence interval [CI] 16.7-41.5 nM) and inhibition constant (K_i) of 12.3 nM (95% CI 7.8-19.4 nM) for WL12. FPy-WL12 exhibited an IC_{50} of 31.7 nM (95% CI 20.7-48.6 nM) and K_i of 14.8 nM (95% CI 9.7-22.7 nM). The results demonstrate that WL12 retains high binding affinity to PD-L1 after acylation of δ -amine of ornithine.

[^{18}F]FPy-WL12 Shows PD-L1 Specific In Vitro Cellular Uptake

Flow cytometry analysis showed that the selected cell lines exhibit a range of cell surface PD-L1 expression in the order: hPDL1>MDAMB231>H226>SUM149>H1155>CHO (Figure 1C and D). Reflecting the flow cytometry data, a high [^{18}F]FPy-WL12 uptake was observed in PD-L1-positive hPD-L1, MDAMB231, and H226 cells compared to PD-L1-negative CHO, SUM149, and H1155 cells (Figure 1E). Confirming radiotracer specificity, [^{18}F]FPy-WL12 uptake was significantly reduced in cells coincubated with unmodified WL12 ($P > 0.001$). Collectively, these studies demonstrate the in vitro specificity of [^{18}F]FPy-WL12 for PD-L1.

PD-L1 Expression-Dependent In Vivo Accumulation of [^{18}F]FPy-WL12 in Different Tumor Models

We assessed the biodistribution and pharmacokinetics of [^{18}F]FPy-WL12 by PET imaging and ex vivo biodistribution studies in NSG mice bearing CHO xenografts with high and low PD-L1 expression (Figure 2). The PET-CT images of mice showed significantly higher accumulation of [^{18}F]FPy-WL12 in hPD-L1 tumors compared to CHO controls at 10, 30, and 60 minutes after the radiotracer injection (Figure 2A). Confirming the in vivo specificity of [^{18}F]FPy-WL12, a significant reduction in radioactivity uptake was observed in hPD-L1 tumors in mice receiving a blocking dose of unmodified WL12. In addition to hPD-L1 tumors, high radioactivity accumulation was also observed in liver and kidneys.

We performed ex vivo biodistribution studies in mice with the same tumor models to validate the PET imaging observations. [^{18}F]FPy-WL12 uptake in the hPD-L1 tumors was high with %ID/g values of 5.23 ± 1.11 , 7.16 ± 1.67 and 8.86 ± 10.2 at 10, 60, and 120 minutes, respectively. In contrast,

control CHO tumor uptake is less than 1.77 ± 0.21 %ID/g at the same time points (Figure 2B). PD-L1-specific accumulation of [^{18}F]FPy-WL12 resulted in high tumor-to-muscle and tumor-to-blood ratios (Figure 2B). The [^{18}F]FPy-WL12 uptake in hPD-L1 tumors was significantly reduced ($P < 0.001$) in mice that received a blocking dose of WL12. We observed an 85% (1.29 ± 0.18 %ID/g) reduction in the uptake of [^{18}F]FPy-WL12 in hPD-L1 tumors, while no significant differences were observed in control CHO tumors. Immunohistochemical analysis of tumors for PD-L1 showed intense immunoreactivity in hPD-L1 tumors and not in CHO tumors, confirming PD-L1 expression in the tumors (Figure 2C). These results confirmed that [^{18}F]FPy-WL12 uptake in hPD-L1 tumors is indeed PD-L1 specific.

In addition to hPD-L1 tumors, high accumulation of [^{18}F]FPy-WL12 was observed in liver and kidneys at all the time points. A blocking dose had minimal effect on the [^{18}F]FPy-WL12 uptake in those tissues, suggesting a nonspecific accumulation of the radiotracer. Overall, high image contrast with [^{18}F]FPy-WL12 was observed at 120 minutes. Thus, imaging and biodistribution studies in other tumor models were performed at 120 minutes to take advantage of the observed high tumor-to-muscle (and blood) and hPD-L1-to-CHO tumor ratios.

We next evaluated PD-L1 specificity of [^{18}F]FPy-WL12 in mice bearing MDAMB231 TNBC xenografts with moderate levels of endogenous PD-L1 expression. The PET-CT images of those mice indicated modest accumulation of radioactivity in MDAMB231 tumors (Figure 3A).

In the biodistribution studies, accumulation of [^{18}F]FPy-WL12 in MDAMB231 tumors reached 2.15 ± 0.1 %ID/g at 120 minutes. Upon co-injection of [^{18}F]FPy-WL12 with WL12, radioactivity accumulation in MDAMB231 tumors was reduced to 0.81 ± 0.063 %ID/g confirming radiotracer specificity (Figure 3B). To further validate the PD-L1 specificity, we performed biodistribution studies in mice with SUM149 tumors that have low PD-L1 expression.^{8,20} [^{18}F]FPy-WL12 accumulation was low in SUM149 tumors at 1.43 ± 0.11 %ID/g ($P < .001$). Immunohistochemical analysis of tumors for PD-L1 expression showed high immunoreactivity in MDAMB231 tumors and low immunoreactivity in SUM149 tumors (Figure 3C), providing further evidence that observed radiotracer uptake is PD-L1 specific.

We also evaluated [^{18}F]FPy-WL12 uptake in the lung squamous cell carcinoma H226 xenograft model (Figure 4). The PET-CT and ex vivo biodistribution studies showed a 2.77 ± 0.31 %ID/g of radioactivity accumulation in H226 tumors at 2 hours after radiotracer injection (Figure 4A). A blocking dose of WL12 co-injected with the radiotracer resulted in reduced [^{18}F]FPy-WL12 uptake in H226 tumors (1.28 ± 0.13 %ID/g), validating the results observed in breast cancer xenografts (Figure 4B). The IHC analysis of tumors showed moderate immunoreactivity for PD-L1 (Figure 4C). Collectively, these results validated the PD-L1 specificity of [^{18}F]FPy-WL12 in tumor models with endogenous PD-L1 expression.

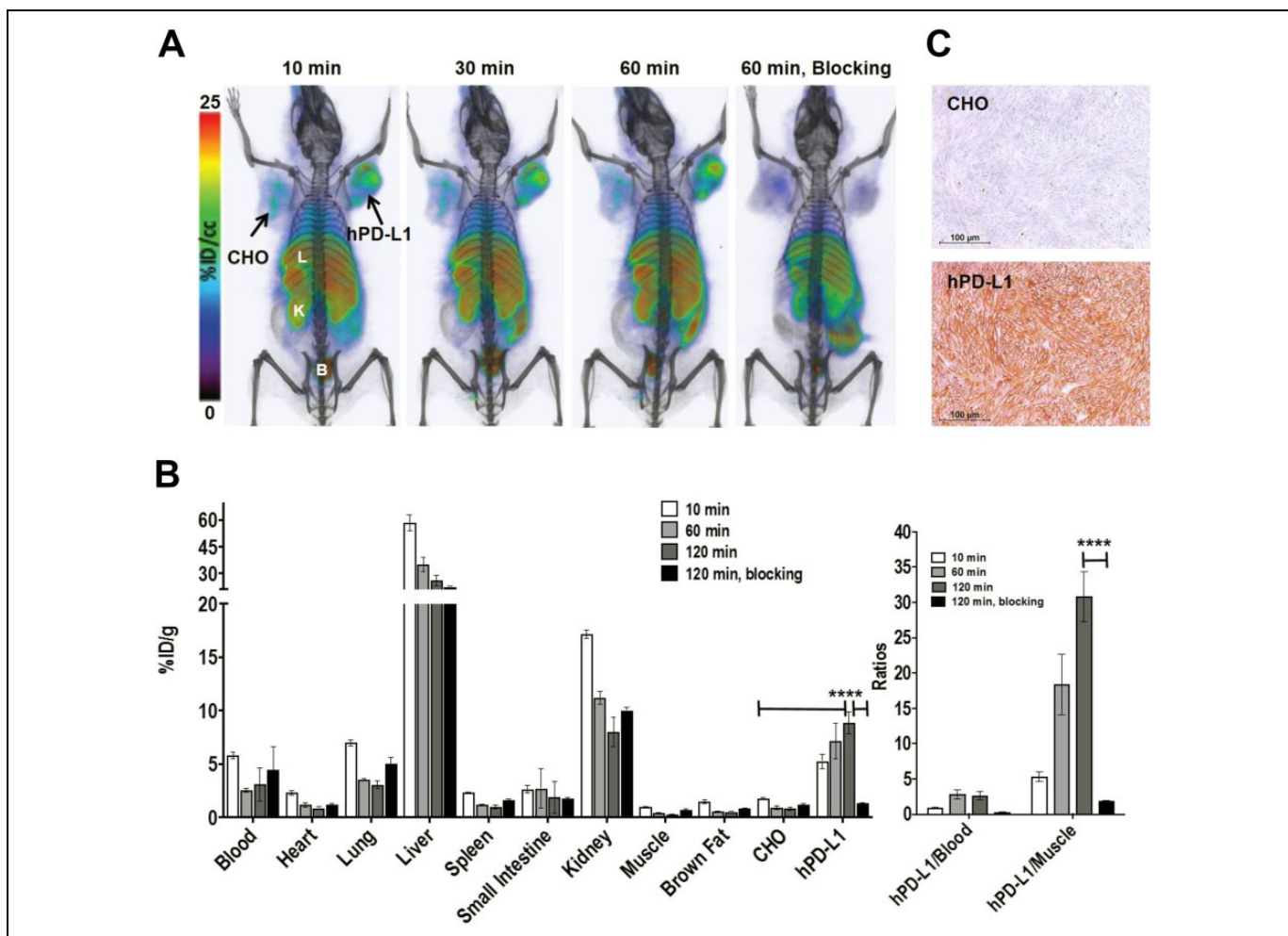


Figure 2. Detection of PD-L1 expression in subcutaneous CHO xenografts with [^{18}F]FPy-WL12. **A**, The 3D volume rendered whole-body PET/CT images demonstrate specific accumulation of activity in the hPD-L1 but not in control CHO tumors ($n = 3$). NSG mice with CHO and CHO-hPD-L1 xenografts were administered intravenously with 7.4 MBq (200 μCi) of [^{18}F]FPy-WL12 and imaged 10, 30, and 60 minutes post radiotracer injection. **B**, Ex vivo biodistribution analysis of the [^{18}F]FPy-WL12 at 10, 60, and 120 minutes after the radiotracer injection, indicating specific uptake of [^{18}F]FPy-WL12 by hPD-L1 tumors ($n = 4/\text{time point}$) **** $P < 0.001$. NSG mice bearing CHO and hPD-L1 subcutaneous tumors were administered intravenously with 1.48 MBq (40 μCi) of [^{18}F]FPy-WL12 and dissected at above-specified time points, followed by analysis of the obtained samples on a γ counter. Results are expressed as percentage of injected dose per gram of tissue (%ID/g). For blocking experiments, [^{18}F]FPy-WL12 was coinjected with 50 μg of unmodified peptide, *** $P < 0.01$. **C**, Immunohistochemical analysis for PD-L1 expression demonstrating intense immunoreactivity in hPD-L1 tumors compared to CHO tumors.

Discussion

Here we report the preparation and evaluation of an [^{18}F]-radiolabeled PD-L1-binding peptide, [^{18}F]FPy-WL12, and demonstrated the PD-L1 specificity of the radiotracer in vitro and in vivo in several human cancer xenografts.

In a recent study, we demonstrated that a ^{64}Cu -labeled DOTAGA-WL12 conjugate provides high-contrast PET images of tumor PD-L1 expression in mouse models within 120 minutes.¹⁵ Considering the rapid and specific uptake of [^{64}Cu]WL12 in PD-L1-positive tumors, we hypothesized that an ^{18}F -labeled WL12 analog would be more desirable for PET imaging. Fluorine-18 is well suited for clinical translation with 97% decay via positron emission and a 109.77-minute half-life

that allows transportation of the radiotracer from the regional radiopharmacy to the clinical site.

With the exception of Al ^{18}F labeling of polyaminocarboxylate conjugates, ^{18}F -labeled peptides are usually prepared by conjugation of an ^{18}F -labeled prosthetic group, many of which require multi-step radiosyntheses. Olberg et al reported a convenient 1-step radiosynthesis of the prosthetic group 2,3,5,6-tetrafluorophenyl-6-[^{18}F]fluoronicotinate ([^{18}F]FPy-TFP) that was further simplified by a resin-based labeling approach by Basuli et al.^{11,12,18} Taking advantage of that 1-step approach, we prepared [^{18}F]FPy-WL12 by the conjugation of [^{18}F]FPy-TFP to WL12 in high radiochemical purity (>95%), modest radiochemical yield, and specific activity. The low overall

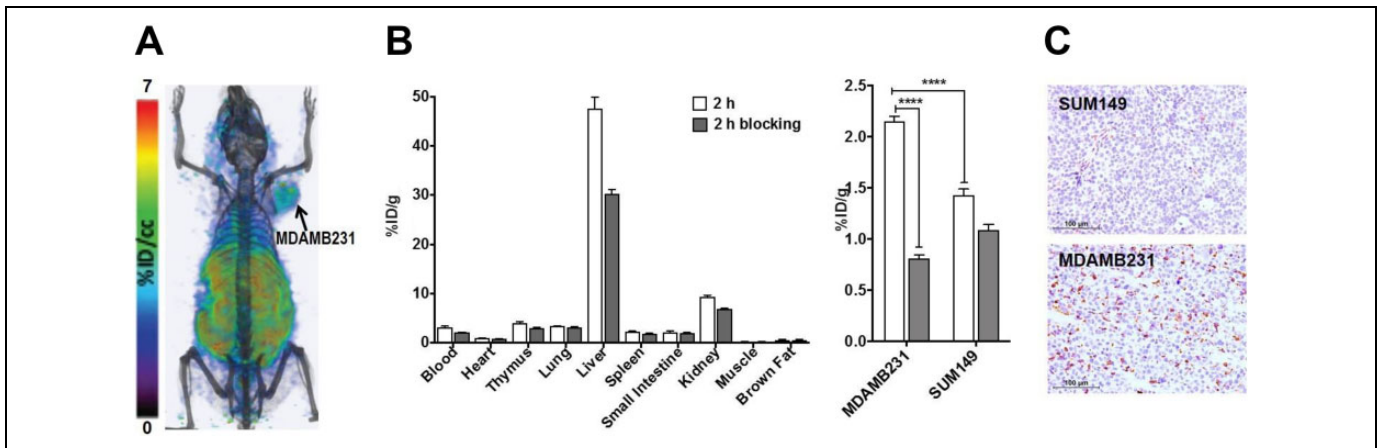


Figure 3. Evaluation of $[^{18}\text{F}]\text{FPy-WL12}$ in mice bearing MDAMB231 and SUM149 TNBC xenografts. A, Volume-rendered PET-CT image of a mouse with MDAMB231 tumor, collected 2 hours after 7.4 MBq (200 μCi) of $[^{18}\text{F}]\text{FPy-WL12}$ injection, indicating radioactivity uptake in the tumor ($n = 3$). B, Ex vivo biodistribution analysis of $[^{18}\text{F}]\text{FPy-WL12}$ at 2 hours after injection in mice bearing MDAMB231 and SUM149 tumors ($n = 4/\text{time point}$), demonstrating PD-L1-mediated accumulation of $[^{18}\text{F}]\text{FPy-WL12}$ in the MDAMB231 tumors. For blocking experiments, $[^{18}\text{F}]\text{FPy-WL12}$ was co-injected with 50 μg of unmodified peptide, **** $P < 0.001$; C, Immunohistochemical analysis for PD-L1 expression shows high immunoreactivity in MDAMB231 tumors compared to SUM149 tumors but significantly lower compared to hPD-L1 xenografts.

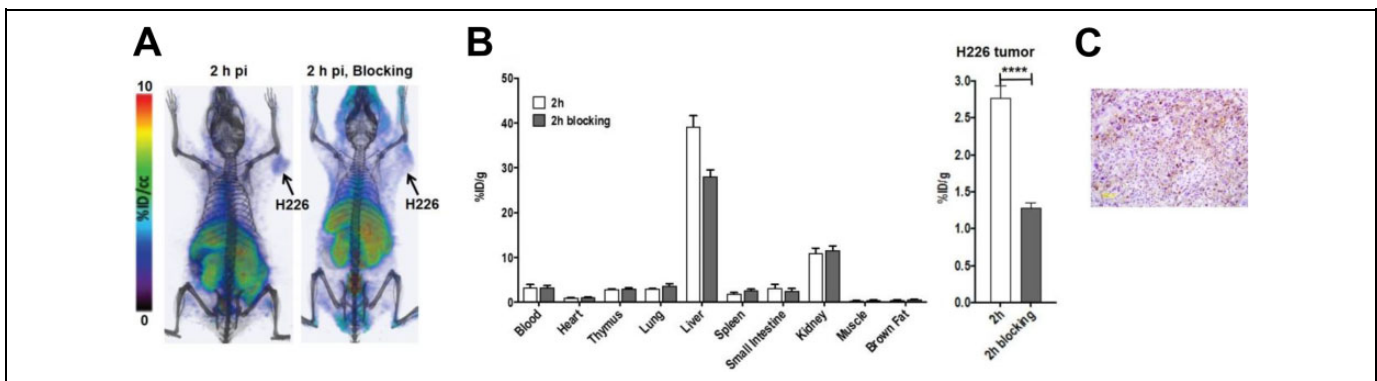


Figure 4. Evaluation of $[^{18}\text{F}]\text{FPy-WL12}$ in H226 lung metastatic squamous cell carcinoma model. A, PET-CT volume-rendered images of $[^{18}\text{F}]\text{FPy-WL12}$ in H226 tumor bearing mice ($n = 3$), demonstrating accumulation of radioactivity in the tumors. B, Ex vivo biodistribution analysis of $[^{18}\text{F}]\text{FPy-WL12}$ at 1 and 2 hours after injection, indicating specific radiotracer accumulation in H226 tumors. For blocking experiments, $[^{18}\text{F}]\text{FPy-WL12}$ was co-injected with 50 μg of unmodified peptide, **** $P < 0.001$. C, Immunohistochemical analysis for PD-L1 expression illustrating low immunoreactivity in H226 tumors.

radiochemical yield ($5.1 \pm 3.1\%$) is likely due to the small amount of WL12 (0.1–0.14 mg, 50–70 nM) used in the conjugation step. The average non-decay corrected (nca) yield for the first step (preparation of $[^{18}\text{F}]\text{FPy-TFP}$) was $35\% \pm 9\%$ and that of conjugation step was $14\% \pm 5\%$. We expect that the radiochemical yield of the conjugation step can be improved using a larger amount of WL12. Increasing WL12 would not affect specific activity of the final product when purified by preparative radio-HPLC, as there is a baseline separation between WL12 and $[^{18}\text{F}]\text{FPy-WL12}$. Our low specific activity $3.885 \pm 1.998 \text{ TBq/mM}$ ($105 \pm 54 \text{ Ci/mM}$) is likely due to the low level of ^{18}F used for radiolabeling and the possibility of fluoride exchange occurring during the radiofluorination, where the tetrafluorophenol ester of

$[^{18}\text{F}]\text{FPy-TFP}$ is the source of the non-radioactive fluorine. We anticipate that automation, which would permit the use of higher levels of $[^{18}\text{F}]\text{fluoride}$, would increase the specific activity of the product. Our experience with this convenient and simple synthon indicates a wide applicability of this radiolabeling strategy for preparing fluorine-18 labeled PD-L1 binding and other peptide imaging agents.

The WL12 is a first-in-class peptide-based imaging agent that enables PD-L1 detection in vivo. To take advantage of rapid pharmacokinetics often associated with peptides and to facilitate the clinical translation of WL12, we pursued radiolabeling strategies with several radionuclides. The potential of WL12 to provide high-contrast images was apparent with DOTAGA-conjugated $[^{64}\text{Cu}]\text{WL12}$.¹⁵ The same analog

radiolabeled with [^{68}Ga], a convenient generator produced radionuclide for clinical translation, showed increased clearance from tissues and provided images with contrast superior to that of [^{64}Cu]WL12.¹⁶ Reflecting the renal clearance associated with peptides, highest uptake is seen in the kidneys with both [^{64}Cu] and [^{68}Ga]WL12 analogs. The high hepatic uptake observed with [^{64}Cu]WL12, but not with [^{68}Ga]WL12, could be due to transchelation of copper that is commonly observed with ^{64}Cu imaging agents.²¹ In contrast to those analogs, the hydrophilicity afforded by the carboxylates is replaced by the less hydrophilic nicotinic group used for fluorination in [^{18}F]FPy-WL12. The influence of lipophilicity on the in vivo distribution of WL12 analogs is clearly evident with the increased hepatic, renal, and normal tissue uptake observed with [^{18}F]FPy-WL12. The low specific activity of [^{18}F]FPy-WL12 could be another contributing factor to the low tumor and high normal tissue uptake observed. While [^{18}F]FPy-WL12 in vivo distribution limits its potential for clinical translation, the observations from our studies provide insights into the influence of the chelator on the pharmacokinetics of a peptide. The advantage of small peptides and the potential to modify their biodistribution were evident in the different pharmacokinetics and image contrast shown by [^{64}Cu], [^{68}Ga], and [^{18}F]Pyl-labeled WL12 peptide and hence the opportunities to improve image contrast using a suitable conjugation and radionuclide labeling method.

Conclusions

In this study, we demonstrated that WL12 can be successfully radiolabeled with [^{18}F] using an fluorine-18 labeled prosthetic group in a procedure that is amenable to automation. The resulting [^{18}F]FPy-WL12 exhibited high affinity to PD-L1 and showed PD-L1 dependent in vitro cellular uptake. [^{18}F]FPy-WL12 demonstrated PD-L1 specific uptake in multiple tumors of various cancer types in PET-CT imaging and ex vivo biodistribution studies. However, it is possible that WL12 when radiolabeled with F-18 using Al ^{18}F chelation methods may produce the improved pharmacokinetics similar to those previously reported for ^{68}Ga - and ^{64}Cu -labeled WL12 due to decreased lipophilicity and off-target uptake.

Author Contribution

Wojciech G. Lesniak and Ronnie C. Mease contributed equally.

Declaration of Conflicting Interests

The author(s) declared no potential conflicts of interest with respect to the research, authorship, and/or publication of this article.

Funding

The author(s) disclosed receipt of the following financial support for the research, authorship, and/or publication of this article: This work was supported by the US National Institutes of Health grants R01CA16631, R01CA236616, P30CA006973, and P41EB024495.

ORCID iD

Sridhar Nimmagadda  <https://orcid.org/0000-0002-6413-7191>

Supplemental Material

Supplemental material for this article is available online.

References

- Chen DS, Mellman I. Oncology meets immunology: the cancer-immunity cycle. *Immunity*. 2013;39(1):1–10.
- Topalian SL, Taube JM, Anders RA, Pardoll DM. Mechanism-driven biomarkers to guide immune checkpoint blockade in cancer therapy. *Nat Rev Cancer*. 2016;16(5):275–287.
- Patel SP, Kurzrock R. PD-L1 expression as a predictive biomarker in cancer immunotherapy. *Mol Cancer Ther*. 2015;14(4):847–856.
- Rehman JA, Han G, Carvajal-Hausdorf DE, et al. Quantitative and pathologist-read comparison of the heterogeneity of programmed death-ligand 1 (PD-L1) expression in non-small cell lung cancer. *Modern Pathol*. 2017;30(3):340–349.
- Weissleder R, Schwaiger MC, Gambhir SS, Hricak H. Imaging approaches to optimize molecular therapies. *Sci Transl Med*. 2016;8(355):355ps16.
- Heskamp S, Hobo W, Molkenboer-Kuenen JD, Olive D, Oyen WJ, Dolstra H, Boerman OC. Noninvasive imaging of tumor PD-L1 expression using radiolabeled anti-PD-L1 antibodies. *Cancer Res*. 2015;75(14):2928–2936.
- Josefsson A, Nedrow JR, Park S, et al. Imaging, biodistribution, and dosimetry of radionuclide-labeled PD-L1 antibody in an immunocompetent mouse model of breast cancer. *Cancer Res*. 2016;76(2):472–479.
- Chatterjee S, Lesniak WG, Gabrielson M, et al. A humanized antibody for imaging immune checkpoint ligand PD-L1 expression in tumors. *Oncotarget*. 2016;7(9):10215–10227.
- Truillet C, Oh HJ, Yeo SP, et al. Imaging PD-L1 expression with immunoPET. *Bioconjug Chem*. 2017;29(1):96–103.
- Hettich M, Braun F, Bartholoma MD, Schirmbeck R, Niedermann G. High-resolution PET imaging with therapeutic antibody-based PD-1/PD-L1 checkpoint tracers. *Theranostics*. 2016;6(10):1629–1640.
- Bensch F, van der Veen EL, Lub-de Hooge MN, et al. (89)Zr-atezolizumab imaging as a non-invasive approach to assess clinical response to PD-L1 blockade in cancer. *Nat Med*. 2018;24(12):1852–1858.
- Maute RL, Gordon SR, Mayer AT, et al. Engineering high-affinity PD-1 variants for optimized immunotherapy and immuno-PET imaging. *P Natl Acad Sci USA*. 2015;112(47):E6506–E6514.
- Donnelly DJ, Smith RA, Morin P, et al. Synthesis and biologic evaluation of a novel F-18-labeled adnectin as a PET radioligand for imaging PD-L1 expression. *J Nucl Med*. 2018;59(3):529–535.
- Niemeijer AN, Leung D, Huisman MC, et al. Whole body PD-1 and PD-L1 positron emission tomography in patients with non-small-cell lung cancer. *Nat Commun*. 2018;9(1):4664.

15. Chatterjee S, Lesniak WG, Miller MS, et al. Rapid PD-L1 detection in tumors with PET using a highly specific peptide. *Biochem Biophys Res Commun*. 2017;483(1):258–263.
16. De Silva RA, Kumar D, Lisok A, et al. Peptide-based (68)Ga-PET radiotracer for imaging PD-L1 expression in cancer. *Mol Pharm*. 2018;15(9):3946–3952.
17. Kumar D, Lisok A, Dahmane E, et al. Peptide-based PET quantifies target engagement of PD-L1 therapeutics. *J Clin Invest*. 2018. doi: 10.1172/JCI122216.
18. Olberg DE, Arukwe JM, Grace D, et al. One step radiosynthesis of 6-[F-18]fluoronicotinic acid 2,3,5,6- tetrafluorophenyl ester ([F-18]F-Py-TFP): a new prosthetic group for efficient labeling of biomolecules with fluorine-18. *J Med Chem*. 2010;53(4):1732–1740.
19. Basuli F, Zhang X, Jagoda EM, Choyke PL, Swenson RE. Facile room temperature synthesis of fluorine-18 labeled fluoronicotinic acid-2,3,5,6-tetrafluorophenyl ester without azeotropic drying of fluorine-18. *Nucl Med Biol*. 2016;43(12):770–772.
20. Lesniak WG, Chatterjee S, Gabrielson M, et al. PD-L1 detection in tumors using [Cu-64]atezolizumab with PET. *Bioconjugate Chem*. 2016;27(9):2103–2110.
21. Boswell CA, Sun XK, Niu WJ, et al. Comparative in vivo stability of copper-64-labeled cross-bridged and conventional tetraazamacrocyclic complexes. *J Med Chem*. 2004;47(6):1465–1474.